Mg^{2+}-Dependent Compaction and Folding of Yeast $tRNA^{Phe}$ and the Catalytic Domain of the *B. subtilis* RNase P RNA Determined by Small-Angle X-ray Scattering†

Xingwang Fang,‡ Kenneth Littrell,§ Xiao-jing Yang,‡ Stephen J. Henderson,|| Sonke Siefert,§ P. Thiyagarajan,§ Tao Pan,*,‡ and Tobin R. Sosnick*,‡

Department of Biochemistry & Molecular Biology, University of Chicago, 920 East 58th Street, Chicago, Illinois 60637, Argonne National Laboratory, 9700 South Cass Avenue, Argonne, Illinois 60439, and Department of Physics, University of Colorado, Boulder, Colorado 80309

Received March 30, 2000; Revised Manuscript Received June 23, 2000

ABSTRACT: We apply synchrotron-based small-angle X-ray scattering to investigate the relationship between compaction, metal binding, and structure formation of two RNAs at 37 °C: the 76 nucleotide yeast $tRNA^{Phe}$ and the 255 nucleotide catalytic domain of the *Bacillus subtilis* RNase P RNA. For both RNAs, this method provides direct evidence for the population of a distinct folding intermediate. The relative compaction between the intermediate and the native state does not correlate with the size of the RNA but does correlate well with the amount of surface burial as quantified previously by the urea-dependent *m*-value. The total compaction process can be described in two major stages. Starting from a completely unfolded state (4−8 M urea, no Mg^{2+}), the major amount of compaction occurs upon the dilution of the denaturant and the addition of micromolar amounts of Mg^{2+} to form the intermediate. The native state forms in a single transition from the intermediate state upon cooperative binding of three to four Mg^{2+} ions. The characterization of this intermediate by small-angle X-ray scattering lends strong support for the cooperative Mg^{2+}-binding model to describe the stability of a tertiary RNA.

Proteins and certain RNAs, such as ribozymes, adopt well-defined tertiary structures that are essential for their biological function. How these tertiary structures form from the denatured state has proven remarkably difficult to understand. When tertiary RNAs compact in their Mg^{2+}-dependent, thermodynamic folding pathway is unclear. Collapse of the negatively charged phosphate backbone is electrostatically unfavorable, and folding to the native structure requires charge neutralization by cations. The compaction of a tertiary RNA can be envisioned to occur in at least two stages. The formation of independently stable secondary structure brings unstructured regions into close proximity. Formation of the tertiary structure brings secondary structural motifs together. Actual experimental information, however, is sparse on the relationship between compaction and other processes in tertiary RNA folding.

Small-angle X-ray scattering (SAXS)[1] can determine the dimensions of macromolecules in solution as described by the radius of gyration, R_g, and the $P(r)$ function (*1*−*5*). The $P(r)$ function contains shape information and is the probability distribution of vector lengths within the particle. SAXS is particularly useful for the characterization of unfolded and partially folded states that are not readily studied by high-resolution techniques such as NMR or crystallography. SAXS also is an effective technique to follow changes in size and shape accompanying folding transitions (*6*−*15*). Furthermore, SAXS is well-suited for the study of RNAs due to their ∼5-fold increase in scattering signal over that of proteins (*3*). This increase in signal is the result of an increase in electronic density difference, or X-ray contrast, between the denser RNA and the aqueous solvent. Although SAXS has been frequently applied to protein folding studies, its potential in RNA folding studies has yet to be fully explored.

Here we apply SAXS to determine the physical compaction of yeast $tRNA^{Phe}$ and the catalytic domain (C-domain) of the *B. subtilis* RNase P RNA during Mg^{2+}-dependent folding to their biological relevant forms. These studies are conducted at relatively low (micromolar) RNA concentrations at the Advanced Photon Source (APS) synchrotron at

† This work is supported by grants from the NIH (R01GM57880 to T.P. and T.R.S.), The U.S. Department of Energy, BES-Materials Science, under Contract W-31-109-ENG-38 (P.T.), The University of Chicago−Argonne National Laboratory Collaborative Seed Grant Program (T.R.S. and P.T.), and the Packard Foundation Interdisciplinary Science Program (T.R.S. and P.T.). BioCat is an NIH-supported Research Center (RR08630).

* Corresponding authors. Telephone: (773)834-0657; Fax: (773)-702-0439; E-mail: taopan@midway.uchicago.edu, trsosnic@midway.uchicago.edu.

‡ University of Chicago.

§ Argonne National Laboratory.

|| University of Colorado.

[1] Abbreviations: *C*, weight concentration (in mg/mL); C-domain, catalytic domain of the *B. subtilis* RNase P RNA containing nucleotides 240−409 + 1−85; d_{max}, maximum distance; K_{Mg}, Mg^{2+} concentration at the midpoint of an RNA folding transition; *m*, free energy dependence of the I-to-N transition on the urea concentration; λ, X-ray wavelength; *n*, Hill constant; $P(r)$, pair distance distribution function; *Q*, scattering vector; R_g, radius of gyration; SAXS, small-angle X-ray scattering; θ, half-scattering angle; U′ (or U_{urea}), unfolded state in 4 M urea ($tRNA^{Phe}$) or 8 M urea (C domain), in the absence of Mg^{2+}.

10.1021/bi000724n CCC: $19.00
Published on Web 08/12/2000

the Argonne National Laboratory. The relationship between compaction and other folding events, the nature of partially folded species, comparisons between the observed and predicted structures, and thermodynamics of tertiary RNA folding are discussed.

MATERIALS AND METHODS

Sample Preparation. RNAs were prepared by in vitro transcription using standard methods (*16*). After transcription, RNA transcripts were precipitated with ethanol, dissolved in 7 M urea, 100 mM EDTA loading buffer, and purified on polyacrylamide gels containing 7 M urea and 2 mM EDTA. The RNAs were eluted from the gel by the crush-and-soak method in 50 mM potassium acetate/200 mM KCl, pH 7, precipitated in ethanol, and stored in water at −20 °C.

In all experiments, the purified RNAs were first heated in 20 mM TrisHCl, pH 8.1, at 85−90 °C for 2 min followed by incubation at ambient temperature for 3 min. The RNA at this stage was designated as the U state.

Small-Angle X-ray Scattering. SAXS experiments were carried out at the SAXS instrument on the BESSRC ID-12 beam-line of Argonne National Laboratory's Advanced Photon Source (*17*). Data were collected using a 9-element (15 cm × 15 cm) mosaic CCD area detector, and exposure times were 1−6 s for each measurement. Sample to detector distance was 3 m, and energy of X-ray radiation was set to 13.5 keV. Computer-controlled Hamilton brand syringes injected sample into a thermostated flow cell made of a 1.5 mm diameter cylindrical quartz capillary of 0.01−0.02 mm wall thickness. The background scattering was from a buffer solution in the identical configuration to enable proper background subtraction. Some measurements were performed at the BIOCAT ID-18 beam-line using the same camera at 8.5 keV. Although the sample to background scattering level for 0.3 mg/mL $tRNA^{Phe}$ was less than 1.1 at $Q < 0.01$ Å, the high number of counts produces data with less than 3% statistical error per data point.

To reduce the possibility of radiation damage, samples were measured under constant flow conditions. Mg^{2+} titrations were performed using a second syringe that added aliquots of concentrated $MgCl_2$ solutions to a 0.5−1 mL sample followed by withdrawal through the quartz capillary.

Radiation Damage. The high flux of X-rays at the APS generates a large number of hydroxyl radicals that can cause secondary radiation damage to RNA [as is applied to RNA tertiary structure footprinting studies (*18*)]. We observed such radiation damage, as indicated by sample aggregation or an increase in the R_g, within 30 s of static exposure in control studies on fully folded, unmodified yeast $tRNA^{Phe}$ in 10 mM Mg^{2+}, 10 mM phosphate, pH 7 (data not shown). Inorganic phosphate, however, is known to be a poor hydroxyl radical scavenger (*19*). Hence, subsequent measurements were performed in TrisHCl buffer that rapidly scavenged hydroxyl radicals. Additionally, experiments were conducted under constant flow conditions to further reduce the possibility of radiation damage. Using these protocols, we observed no radiation damage during the course of the measurements.

Data Analysis. In a SAXS experiment, the X-ray scattering profile is measured at very low scattering angles ($\theta < 3°$). Data are presented as the scattering intensity per solid angle, $I(Q)$, where the scattering vector Q is defined as $Q = 4\pi \sin\theta/\lambda$, λ is the X-ray wavelength, and θ is the half-scattering angle. The dimensions of a particle can be determined from the width of the inner part of the scattering profile which can be approximated as a Gaussian, $I(Q) = I(0)e^{-Q^2R_g^2/3}$. The R_g is the root-mean-square of the distances of all regions to the center-of-mass of the particle. For globular particles, R_g can be obtained with ∼3% accuracy from the slope of ln $I(Q)$ versus Q^2 for $Q \leq 1.3/R_g$ in a Guinier plot (*20, 21*).

More precise structural parameters were derived from a $P(r)$ analysis using the entire scattering profile. The $P(r)$ function has a maximum at the most probable distance in the object (e.g., slightly larger than the radius for a sphere) and goes to zero at the maximum dimension, d_{max}, of the object (e.g., the diameter). $P(r)$ functions were calculated according to

$$P(r) = \frac{1}{2\pi^2}\int_{Q_{min}}^{Q_{max}} I(Q)Qr \sin(Qr)\, dQ \qquad (1)$$

using the indirect Fourier inversion algorithms developed by Moore (*4*) and Svergun (*22*). Results obtained from these two different approaches were nearly identical; however, only the results using the Moore algorithm were presented. The R_g is determined from the second moment of $P(r)$ according to

$$R_g^2 = \frac{\int_0^{d_{max}} r^2 P(r)\, dr}{2\int_0^{d_{max}} P(r)\, dr} \qquad (2)$$

No significant differences were observed for the R_g values determined from the Guinier Plots and from the $P(r)$ analysis.

The scattering at various Mg^{2+} concentrations during the I-to-N transition is from a binary mixture of two equal mass states. Assuming the scattering from each state has the same X-ray contrast and same volume so that each contributes equally to the scattering intensity, the $P(r)$ function is the weighted sum of each of the individual $P(r)$ functions:

$$P(r) = f_I P_I(r) + f_N P_N(r) \qquad (3)$$

where f_I and f_N are the fractions of the I and N states, respectively. The observed R_g^2 from such a mixture is the weighted sum of the R_g^2 for each of the particles:

$$\begin{aligned} R_g^2 &= \frac{\int r^2[f_I P_I(r) + f_N P_N(r)]\, dr}{2\int P(r)\, dr} \\ &= \frac{f_I\int r^2 P_I(r)\, dr + f_N\int r^2 P_N(r)\, dr}{2\int P(r)\, dr} \\ &= f_I R_I^2(r) + f_N R_N^2 \end{aligned} \qquad (4)$$

where R_I and R_N are the R_g values of the I and N states, respectively.

The two Mg^{2+}-dependent transitions were described according to a semi-emperical cooperative binding model:

$$U \xleftrightarrow{K_{Mg}^{UI}, n_1} I \xleftrightarrow{K_{Mg}^{IN}, n_2} N$$

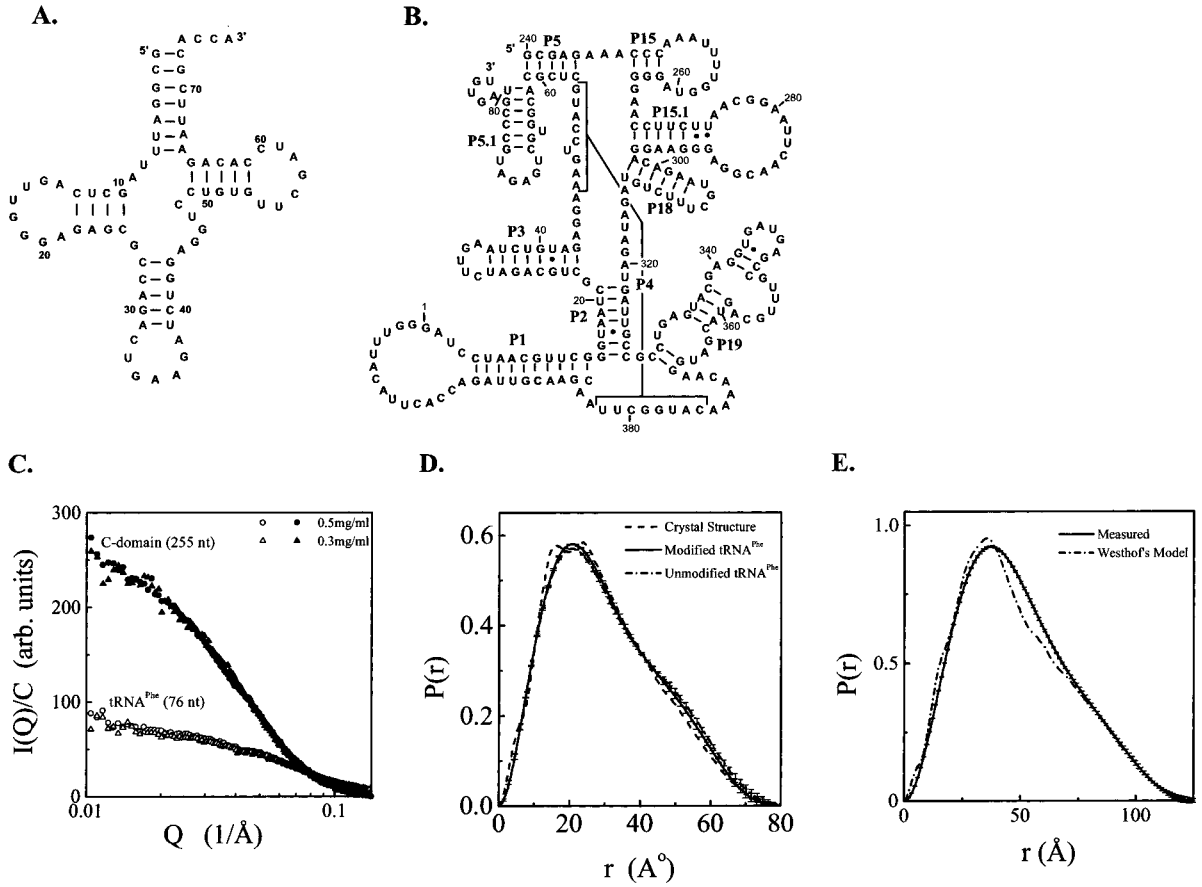

FIGURE 1: Secondary structure representation (A, B) and monodispersity of yeast tRNA^{Phe} and the catalytic domain of the *B. subtilis* RNase P RNA (C−E) (*39*). (C) Scattering profiles normalized to RNA concentration for tRNA^{Phe} (76 nucleotides) and C-domain (255 nucleotides) at 0.3 and 0.5 mg/mL in 10 mM Mg^{2+}, 20 mM TrisHCl, pH 8.1, 37 °C. The overlap for each molecule along with the relative intensities indicates that aggregation and interparticle interference are negligible within this concentration range, and that both RNAs are monodispersed. (D) Comparison of $P(r)$ determined from experiment on the native state of modified ($R_g = 23.5 \pm 0.3$ Å) and unmodified tRNA^{Phe} ($R_g = 23.6 \pm 0.3$ Å), and from the crystal structure ($R_g = 23.5$ Å). (E) Comparison between experimental $P(r)$ function ($R_g = 38.0 \pm 0.5$ Å) with that predicted for the C-domain portion of the Westhof model with an added P1 helix and L1 loop for better comparison to the C-domain construct used in the present study ($R_g = 37.5$ Å).

where n and K_{Mg} are the Hill constant and Mg^{2+} midpoint of each transition, respectively (*23*). Because the two folding transitions in SAXS are sufficiently well-separated, the I-to-N transition can be fit separately for the fraction of fully folded molecules, f_N, according to

$$f_N([Mg^{2+}]) = \frac{[N]}{[I] + [N]} = \frac{[Mg^{2+}]^{n_2}}{[Mg^{2+}]^{n_2} + (K_{Mg}^{IN})^{n_2}} \quad (5)$$

The K_{Mg} and n parameters were used to define the Mg^{2+}-dependent stability. Curve fitting was performed using the Microcal Origin V5.0 nonlinear fitting routine. Listed errors are the standard deviation calculated by the fitting algorithm and reflect the statistical uncertainty of the fitted parameters.

Molecular Modeling. Calculations of $P(r)$ functions from high-resolution structures, either crystal structures or predicted models, were conducted using the program XTL modified for use with nucleic acids (*24*).

The C-domain with the extended P1 and L1 loops was built based on the structural model by Westhof and coworkers (*25*). A total of 17 nucleotides were added as a closing loop connecting C4 and A395 in helix P1. These 17 nucleotides were modeled as an extending stem-loop from P1, which formed an energy-favoring continuous groove surface with the neighboring helix P19. This model was refined by 1000 steps of conjugate gradient refinement.

RESULTS

Monodispersity of Yeast tRNA^{Phe} and C-Domain. SAXS measurements reflect the time and ensemble-averaged structures for molecules in solution. For a monodispersed system, the intensity at zero angle is related to the molecular weight of the scattering species (MW), the RNA weight concentration (C, in mg/mL), and the electron density (ρ) according to (*20*)

$$I(0) \propto (\rho_{RNA} - \rho_{solvent})^2 \times MW \times C \quad (6)$$

Our results (Figure 1C) indicate that tRNA^{Phe} behaves as a monomer based on several lines of evidence. (i) The R_g and the $P(r)$ function of the tRNA^{Phe} are in excellent agreement with those calculated from the crystal structure (Figure 1D). (ii) The R_g values at tRNA concentrations of 0.3−0.5 mg/mL are in agreement with earlier studies conducted over a more extensive concentration range [up to 20 mg/mL (*26, 27*)], including a study where the correct monomolecular weight of tRNA was obtained from the absolute scattering intensity (*28*). (iii) The normalized scattering intensity, $I(0)/C$, is independent of concentration

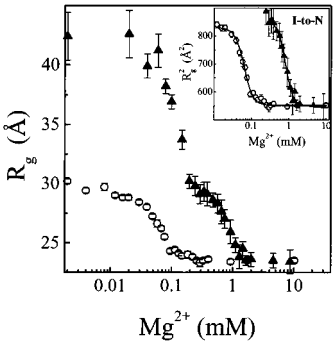

FIGURE 2: Mg^{2+} titration of unmodified $tRNA^{Phe}$ (0.3 mg/mL) in the absence (open circles) and presence (solid triangles) of 4 M urea at 37 °C. Inset: [Mg^{2+}] dependence of R_g^2 for the I-to-N transition. Solid lines are fits to the I-to-N transition using a cooperative Mg^{2+} binding model (eq 5).

for both unmodified (Figure 1C) and modified $tRNA^{Phe}$ (data not shown) at 0.3 and 0.5 mg/mL. The value of $I(0)/C$ should have increased with an increase in the level of aggregation, or decreased if scattering from different particles destructively interferes with scattering from other particles (interparticle interference). Neither of these two effects is significant. For these reasons, we conclude that folded $tRNA^{Phe}$ is a monomer under the experimental conditions, and the average solution structure of $tRNA^{Phe}$ is similar to the crystal structure.

The monodispersity of the C-domain in 10 mM Mg^{2+} is determined by comparison to the scattering intensity of $tRNA^{Phe}$ (Figure 1C). Assuming both RNAs have the same electron density and X-ray contrast, the $I(0)/C$ for each RNA should be proportional to its molecular weight, or approximately the number of nucleotides (eq 6). Based upon $tRNA^{Phe}$ having 76 nucleotides, the effective number of residues of the C-domain is 262 ± 5, very close to the actual value of 255. Furthermore, the normalized scattering profiles, $I(Q)/C$, for the larger RNA are independent of concentration at 0.3 and 0.5 mg/mL.

Although a high-resolution structure of the C-domain is not yet available, three-dimensional models have been proposed by Westhof (*25*) and Pace (*29*) and their coworkers. The $P(r)$ function and R_g calculated from the Westhof model are similar to the experimental data (Figure 1E). The R_g calculated from a similarly modified version of the model proposed by Pace and co-workers is within 0.5 Å of that from the Westhof model.

Mg^{2+}-Dependent Folding of tRNA. (A) Folding Transitions. Changes in the dimension during the Mg^{2+}-induced folding of unmodified $tRNA^{Phe}$ are examined by SAXS in the presence and absence of 4 M urea (Figure 2). In the presence of urea, two distinct folding transitions are indicated by the dependence of R_g on Mg^{2+} concentration. The first, termed U′-to-I, occurs between 0 and 0.2 mM Mg^{2+}, and the second, termed I-to-N, occurs between 0.3 and 2 mM Mg^{2+}. The I state has an R_g of 29 ± 1 Å and completely folds to the native state as Mg^{2+} is increased beyond 2 mM. The native state in 4 M urea has a R_g of 23.5 ± 0.3 Å, identical to the value determined in the absence of urea and calculated from the crystal structure (Figure 1D).

In the absence of urea, the I-to-N transition is clearly evident and occurs between 0.02 and 0.2 mM Mg^{2+}. Little change in the R_g, however, is observed for the U-to-I transition which occurs at Mg^{2+} concentrations below 0.02 mM. This result indicates that even in the absence of Mg^{2+} and urea, the U state of $tRNA^{Phe}$ adopts a structure that is nearly as compact as the I state.

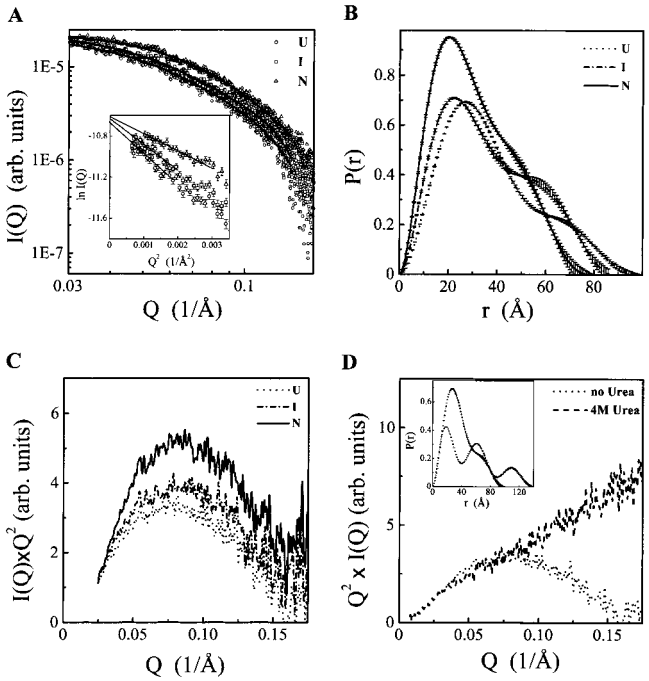

FIGURE 3: U_{urea} (U′), U, I, and N states of unmodified $tRNA^{Phe}$ at 37 °C. (A) The scattering profiles of the U (no Mg^{2+}), I (0.01 mM Mg^{2+}), and N (10 mM Mg^{2+}) states in 20 mM TrisHCl, pH 8.1. Solid lines are the fits to the data using the Moore algorithm. Inset: Guinier plot; solid lines are best fits of the data up to $Q = 1.3/R_g$. (B) $P(r)$, calculated from the fits to the scattering data. (C) Kratky plot. (D) Unfolded state in the absence (U) or presence of 4 M urea (U′). The scattering from U′ has been normalized to the intensity of the other three to account for the change in scattering contrast of the buffer due to the presence of urea.

The value of $I(0)/C$ is constant for the three states in the absence (Figure 3A) and presence of urea (data not shown). This result indicates that there are no significant differences in the monodispersity of these three states.

Our previous folding studies (*30*) of this tRNA can be used as a guideline to quantitatively evaluate the folding transitions observed by SAXS. The thermodynamic folding pathway of $tRNA^{Phe}$ is described with three populated species and two Mg^{2+}-dependent transitions:

$$U \xleftrightarrow{K_{Mg}^{UI}, n_1} I \xleftrightarrow{K_{Mg}^{IN}, n_2} N$$

where n and K_{Mg} are the Hill constant and Mg^{2+} midpoint of each transition, respectively. The values for n and K_{Mg} are determined from the change in R_g^2, rather than R_g, as appropriate for a binary mixture [(*12*) and see Materials and Methods]:

$$R_g^2 = f_I R_I^2 + f_N R_N^2 = (1 - f_N) R_I^2 + f_N R_N^2 \qquad (7)$$

The resulting n and K_{Mg} values for the I-to-N transition are 3.7 ± 0.5 and 0.063 ± 0.003 mM, respectively. A urea-induced unfolding titration identifies a denaturant response parameter, the m-value, that is the amount of destabilization per molar of added denaturant (units of kcal mol^{-1} M^{-1}). The m-value correlates with the amount of surface area

exposed in the unfolding transition of RNA (*30*). In the presence of 4 M urea, the K_{Mg} increases 13-fold (0.81 ± 0.05 mM), while the Hill constant remains unchanged (n = 4.0 ± 0.7). This sensitivity of K_{Mg} to urea indicates that the urea-sensitive surface area is buried in this folding transition (*30*), and this amount equates to an m-value of 1.6 ± 0.1 kcal mol^{-1} M^{-1}.

Both the Hill constant and the m-value determined by SAXS are in excellent agreement with those obtained from circular dichroism and hydroxyl radical protection (*30*). However, the K_{Mg} determined by SAXS is about 3 times higher than that obtained from the previous studies. This difference primarily is due to the 30-fold higher RNA concentration used in the SAXS studies (13 μM versus 0.5 μM), as verified for C-domain folding (see below).

(B) Scattering of the U, I ,and N States. Figure 3 shows the scattering profiles and $P(r)$ functions for the three thermodynamic states. The dimensions of the I (R_g = 29 ± 1 Å; d_{max} ~ 90 Å) and N states (R_g = 23.5 ± 0.3 Å, d_{max} ~ 80 Å) remain unchanged in 0 and 4 M urea. This result suggests that the I state, as well as the N state, is a distinct structural entity and not an ensemble of structures having different dimensions whose population is sensitive to solvent conditions. This interpretation is consistent with our previous studies where minimal spectroscopic difference is observed for each of these two states upon the addition of 4 M urea (*30*).

In contrast, the U state is sensitive to solvent conditions and becomes much more extended in the presence of 4 M urea. The R_g increases from 29 to 43 Å, and the d_{max} from 90 to 130 Å (Figures 2 and 3D). This result indicates that the U state has a considerable amount of residual structure that is disrupted upon the addition of urea. The U (no urea) state, however, represents an ensemble of structures that is continuously disrupted upon the addition of urea, and leads to the U(urea). Because of differences in the U states, the R_g changes by less than 1 Å in the U-to-I transition in the absence of urea, and by 15 Å in the presence of 4 M urea.

A Kratky plot [$Q^2I(Q)$ versus Q] is used to illustrate the differences in compaction between the different conformations of tRNA^{Phe} (Figure 3C,D). In general, scattering from spherical particles at high angle obeys Porod's law and decreases as $I(Q) \propto Q^{-4}$ (*9*). The Kratky trace has a maximum at a Q-value dependent on the size of the particle, and the trace goes to zero at high angles. For extended particles such as coiled chain molecules, the scattering decreases as Q^{-2} at intermediate angles and Q^{-1} at high angles. This behavior results in a plateau followed by an upturned region at high Q in the Kratky plot.

Experimentally for tRNA^{Phe}, the Kratky traces for the $U_{no\ urea}$, I, and N states exhibit a pronounced peak indicating that all three states are reasonably compact. However, the upward trace for the U state in 4 M urea indicates that this species is largely an extended, coil-like structure.

Mg^{2+}-Dependent Folding of the C-Domain. Two transitions are observed by SAXS in the Mg^{2+}-dependent folding of the C-domain (Figure 4). The U-to-I transition occurs between 0 and 1 mM Mg^{2+} and the I-to-N transition between 1 and 6 mM Mg^{2+}. An intermediate is populated at ~1 mM Mg^{2+} and has a R_g value of 46 ± 0.5 Å. The dependence of R_g^2 on Mg^{2+} concentration for the I-to-N transition is analyzed using a Hill-type analysis to obtain a Hill constant

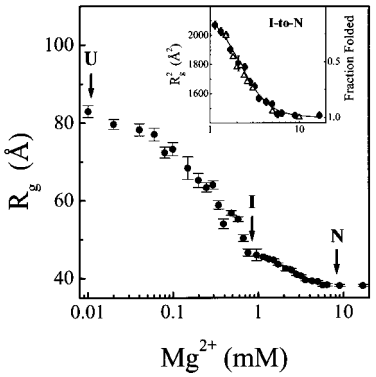

FIGURE 4: Mg^{2+}-induced folding of the C-domain at 0.3 mg/mL, 37 °C, in 20 mM TrisHCl, pH 8.1. Arrows denote the Mg^{2+} concentration where the U, I, or N state dominates. Inset: Mg^{2+} binding plot of R_g^2 for the I-to-N transition. Solid line is the fit using a cooperative Mg^{2+} binding model (eq 5). The open triangles show the folded fraction determined by hydroxyl radical protection at the same RNA concentration.

of 2.7 ± 0.4 and a K_{Mg} of 2.2 ± 0.5 mM. Just like tRNA^{Phe}, the Hill constant of the C determined by SAXS is identical to that obtained by spectroscopy, hydroxyl radical protection, and catalytic activity (*31, 32*). The nearly 2-fold higher K_{Mg} value is due to the higher RNA concentration used in the SAXS experiments (3.8 μM) compared to that used in our previous studies (0.2 μM). The I-to-N transition at 3.8 μM RNA monitored by hydroxyl radical protection (Figure 4, inset) is identical to this transition determined by SAXS. Presumably, the higher RNA concentration reduces the free Mg^{2+} concentration through nonspecific binding (*33, 34*), resulting in an increase in the apparent K_{Mg}.

The $P(r)$ analysis and Kratky plots (Figure 5) indicate that the I and N states of the C-domain are quite compact and have similar dimensions. In contrast, the U state is extended with its Kratky trace exhibiting a mild hump with characteristics of both a compact and an extended particle. This behavior suggests that the U state may be composed of regions of structure connected by extended regions. This residual structure is disrupted by the addition of 8 M urea and 4 mM EDTA to result in an increase in R_g from 80 ± 2 to 180 ± 10 Å and in d_{max} from ~225 to ~450 Å (Figure 5D).

DISCUSSION

Compaction and RNA Folding Transitions. Based upon the present results for tRNA^{Phe} and the C-domain, we propose that the compaction for tertiary RNA folding can be thought of as a two-stage event (Figure 6). Starting from a completely unfolded state in 4−8 M urea in the absence of Mg^{2+} (U′ state), the first compaction event occurs upon the dilution of urea and/or the addition of Mg^{2+}. This stage of compaction generates a distinct intermediate (I state). The detection of this intermediate by SAXS corroborates well with our previous spectroscopic studies of these RNAs. Starting from this intermediate, the second compaction event occurs upon the addition of more Mg^{2+}. This stage of compaction generates the native state (N state). Again, SAXS results correlate well with the I-to-N folding transition characterized previously by spectroscopic methods and by chemical modification (*30, 32*).

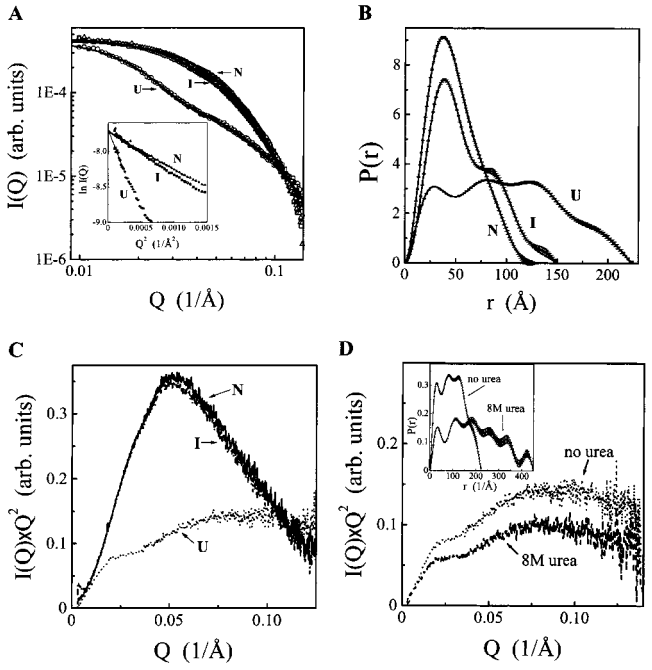

FIGURE 5: The U′, U, I, and N states of the C-domain at 37 °C in 20 mM TrisHCl, pH 8.1. (A) Scattering profiles and fits for the U (no Mg^{2+}), I (0.9 mM Mg^{2+}), and N states (10 mM Mg^{2+}) at 0.5 mg/mL. Inset: Guinier plot; solid lines are best fits of the data up to $Q = 1.3/R_g$. (B) $P(r)$. (C) Kratky plots. The scattering from the U′ has been normalized to the intensity of the other three to account for the change in scattering contrast of the buffer due to the presence of urea.

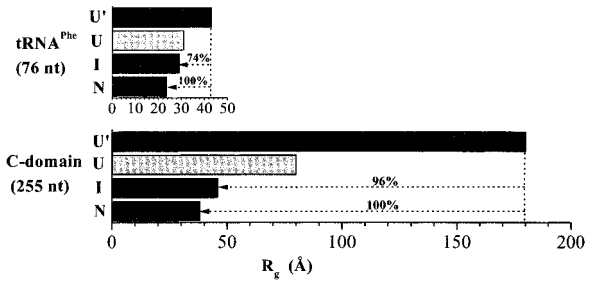

FIGURE 6: Dimensions of thermodynamic states of $tRNA^{Phe}$ and the C-domain. U′ represents the unfolded state in the presence of 4 and 8 M urea for $tRNA^{Phe}$ and the C-domain, respectively. U represents the unfolded state in the absence of Mg^{2+}.

The degree of compaction may be described by the normalized ratio of the R_g values of the U′, I, and N states (Figure 6). For the yeast $tRNA^{Phe}$ and the C-domain, the I state is ~74% and ~96% compact compared to the N state, respectively. This comparison suggests that the I state of the C-domain is relatively more structured compared to the I state of $tRNA^{Phe}$ even though the C-domain has 3.4 times more residues.

The difference in the degree of compaction for the I-to-N transition of these two RNAs is consistent with the difference in their urea *m*-values and spectral properties (*30, 32*). The *m*-value correlates with the amount of surface buried in a folding transition. For the C-domain, the *m*-value is 1.0 kcal mol^{-1} M^{-1}, significantly smaller than the *m*-value for $tRNA^{Phe}$, 1.7 kcal mol^{-1} M^{-1}. In relative terms, the *m*-value for the I-to-N transition of the C-domain is only about 10% of the total for folding starting from a completely unstructured state [estimated by assuming total *m*-value scales linearly with RNA size (*30*)]. In contrast, the *m*-value for the I-to-N transition of $tRNA^{Phe}$ is about 60% of the total *m*-value. No UV absorbance change is observed in the I-to-N transition for the C-domain, suggesting that its I state contains a native amount of secondary structure. In contrast, a significant change in UV absorbance is observed for the I-to-N transition of $tRNA^{Phe}$ (V. Shelton, unpublished results).

It should be noted that the R_g and $P(r)$ functions of both I and N states of $tRNA^{Phe}$ remain the same in 0 and 4 M urea and do not change with Mg^{2+} concentration. This result is consistent with both states being distinct structural entities rather than ensembles of structures having different dimensions and variable amounts of surface burial. The existence of a physically defined I state supports the use of this I state as a thermodynamic reference point for defining tertiary RNA stability.

In contrast to the I and N states, the U state for both RNAs characterized by SAXS is very sensitive to solvent conditions. The addition of urea disrupts residual structure and results in an increase in dimension. This effect is most dramatic for $tRNA^{Phe}$ where in the absence of urea, the U state is nearly as compact as the I state. The extreme sensitivity of the U state to solvent conditions suggests that the U state arises from overlapping and independent structural formation starting from the U′ state. It is likely that until the solvent condition favors the formation of the I state, the U state is composed of a multitude of RNA structures.

The time scales for the folding transitions here may be estimated from previous kinetic studies on the $tRNA^{Phe}$ (*35*), the C-domain (*32*), and other tertiary RNAs. Our stopped-flow absorbance and CD studies have shown that the U-to-I transition for the whole length P RNA at 37 °C occurs on the submillisecond time-scale (*36*). Hence, for both RNAs studied here, the U-to-I transition probably occurs on the submillisecond range as well. The I-to-N transition for these RNAs probably occurs in a time range of 10−100 ms at 37 °C. Starting from the U state, the C-domain folds along a sequential pathway, and there is no evidence that the highly collapsed I state needs to undo structure in order to continue folding. These estimates suggest that the compaction of tertiary RNAs can be very rapid.

Mg^{2+} and Tertiary RNA Stability. Many tertiary RNAs only fold to their biologically relevant conformations in the presence of divalent cations, typically Mg^{2+}. Two types of Mg^{2+}−RNA interactions can be considered in a tertiary folding transition: delocalized and specifically bound (*37, 38*). Although delocalized cations preferentially associate with folded RNA structures having increased negative charge density, we have proposed that the stability of the C-domain can be described adequately by the cooperative binding of three specific Mg^{2+} ions in the I-to-N transition (*31*). Further, our kinetic studies have shown that the C-domain folds in discrete steps upon the sequential binding of these specific cations (*32*).

Our proposal that stability can be defined with a cooperative, Hill-type analysis assumes that the interactions are similar between delocalized Mg^{2+} ions with the I and N states, so that the delocalized Mg^{2+} interactions would not appreciably alter the relative equilibrium between the I and N states. This would be the situation if both states have comparable charge density. The similarity in the size of the two states, as measured by SAXS, suggests that they are likely to have similar charge densities. Hence, the cooperative

binding of a few specific Mg^{2+} ions probably is the dominant factor to be considered in C-domain stability (i.e., the N state over I state), and delocalized Mg^{2+}−RNA interactions do not contribute significantly.

In contrast to the C-domain, the I state of $tRNA^{Phe}$ is much less compact. Nevertheless, we have shown that the Mg^{2+}-dependent stability of this tRNA can be described by the cooperative Mg^{2+} binding model as well (*30*). Potentially, the suitability of a specific binding model to this RNA with a less compact intermediate state is due to the much lower levels of Mg^{2+} required to form the native state. Both hydroxyl radical protection (unpublished results) and SAXS show that $tRNA^{Phe}$ is completely folded below 100 μM Mg^{2+} in the absence of urea. Delocalized Mg^{2+} interactions are probably less important at such low Mg^{2+} concentrations. Hence, under these conditions, delocalized Mg^{2+}−RNA interactions probably have little effect on the stability of this tRNA, and the cooperative binding of a few specific cations is the dominant factor.

CONCLUSION

We have used SAXS to measure compaction during Mg^{2+}-induced folding of yeast $tRNA^{Phe}$ and the C-domain of RNase P RNA from a fully denatured state, U′. Upon the dilution of denaturant, but without the addition of cations, the unfolded state forms structure and undergoes a large decrease in dimension. SAXS physically identifies a distinct thermodynamic intermediate for both tertiary RNAs. For $tRNA^{Phe}$, significant amounts of compaction occur in both the U′-to-I and the I-to-N transitions. For the C-domain, however, the vast majority of the compaction occurs in the U′-to-I transition, and the I state is nearly as compact as the native state. Hence, the compaction process can be different and does not necessarily correlate with the size of the RNA.

ACKNOWLEDGMENT

We thank V. Shelton, C. Correll, and B. Golden for helpful discussions.

REFERENCES

1. Kratky, O., and Pilz, I. (1972) *Q. Rev. Biophys. 5*, 481−537.
2. Kratky, O., and Pilz, I. (1978) *Q. Rev. Biophys. 11*, 39−70.
3. Cantor, C., and Schimmel, P. (1980) *Biophysical Chemistry: Part II*, W. H. Freeman and Co., New York.
4. Moore, P. B. (1980) *J. Appl. Crystallgr. 13*, 168−175.
5. Trewhella, J. (1997) *Curr. Opin. Struct. Biol. 7*, 702−708.
6. Engelman, D. M. (1991) *Proc. Natl. Acad. Sci. U.S.A.*
7. Sosnick, T. R., and Trewhella, J. (1992) *Biochemistry 31*, 8329−8335.
8. Lattman, E. E., Fiebig, K. M., and Dill, K. A. (1994) *Biochemistry 33*, 6158−6166.
9. Lattman, E. E. (1994) *Curr. Opin. Struct. Biol. 4*, 87−92.
10. Doniach, S., Bascle, J., Garel, T., and Orland, H. (1995) *J. Mol. Biol. 254*, 960−967.
11. Semisotnov, G. V., Kihara, H., Kotova, N. V., Kimura, K., Amemiya, Y., Wakabayashi, K., Serdyuk, I. N., Timchenko, A. A., Chiba, K., Nikaido, K., Ikura, T., and Kuwajima, K. (1996) *J. Mol. Biol. 262*, 559−574.
12. Chen, L., Hodgson, K. O., and Doniach, S. (1996) *J. Mol. Biol. 261*, 658−671.
13. Plaxco, K. W., Millett, I. S., Segel, D. J., Doniach, S., and Baker, D. (1999) *Nat. Struct. Biol. 6*, 554−556.
14. Pollack, L., Tate, M. W., Darnton, N. C., Knight, J. B., Gruner, S. M., Eaton, W. A., and Austin, R. H. (1999) *Proc. Natl. Acad. Sci. U.S.A. 96*, 10115−10117.
15. Segel, D. J., Eliezer, D., Uversky, V., Fink, A. L., Hodgson, K. O., and Doniach, S. (1999) *Biochemistry 38*, 15352−15359.
16. Milligan, J. F., Groebe, D. R., Witherell, G. W., and Uhlenbeck, O. C. (1987) *Nucleic Acids Res. 15*, 8783−8798.
17. Seifert, S., Winans, R. E., Tiede, D. M., and Thiyagarajan, P. (2000) *J. Appl. Crystallogr.* (in press).
18. Sclavi, B., Woodson, S., Sullivan, M., Chance, M. R., and Brenowitz, M. (1997) *J. Mol. Biol. 266*, 144−159.
19. Buxton, J. P., Greenstock, G. L., Helman, W. P., and Ross, A. B. (1988) *J. Phys. Chem. Ref. Data 17*, 513−886.
20. Glatter, O., and Kratky, O. (1982) *Small-angle X-ray scattering*, Academic Press, London.
21. Henderson, S. J. (1996) *Biophys J. 70*, 1618−1627.
22. Svergun, D., and Semenyuk, A. (2000) *http://www.srs.dl.ac.uk/ncd/computing/manual.gnom.html*.
23. Cantor, C., and Schimmel, P. (1980) *Biophysical Chemistry: Part III*, W. H. Freeman and Co., New York.
24. Thiyagarajan, P., Henderson, S. J., and Joachimiak, A. (1996) *Structure 4*, 79−88.
25. Massire, C., Jaeger, L., and Westhof, E. (1998) *J. Mol. Biol. 279*, 773−793.
26. Pilz, I., Kratky, O., Cramer, F., Haar, F. v. d., and Schlimme, E. (1970) *Eur. J. Biochem. 15*, 401−409.
27. Zaccai, G., and Xian, S. Y. (1988) *Biochemistry 27*, 1316−1320.
28. Pilz, I., Kratky, O., Haar, F. v. d., and Cramer, F. (1971) *Eur. J. Biochem. 18*, 436−441.
29. Chen, J. L., Nolan, J. M., Harris, M. E., and Pace, N. R. (1998) *EMBO J. 17*, 1515−1525.
30. Shelton, V. M., Sosnick, T. R., and Pan, T. (1999) *Biochemistry 38*, 16831−16839.
31. Fang, X., Pan, T., and Sosnick, T. R. (1999) *Biochemistry 38*, 16840−16846.
32. Fang, X., Pan, T., and Sosnick, T. R. (1999) *Nat. Struct. Biol. 6*, 1091−1095.
33. Stein, A., and Crothers, D. M. (1976) *Biochemistry 15*, 157−160.
34. Bina-Stein, M., and Stein, A. (1976) *Biochemistry 15*, 3912−3917.
35. Urbanke, C., Romer, R., and Maass, G. (1975) *Eur. J. Biochem. 55*, 439−444.
36. Pan, T., and Sosnick, T. R. (1997) *Nat. Struct. Biol. 4*, 931−938.
37. Misra, V. K., and Draper, D. E. (1998) *Biopolymers 48*, 113−135.
38. Tinoco, I., Jr., and Bustamante, C. (1999) *J. Mol. Biol. 293*, 271−281.
39. Haas, E. S., Brown, J. W., Pitulle, C., and Pace, N. R. (1994) *Proc. Natl. Acad. Sci. U.S.A. 91*, 2527−2531.

BI000724N